ACS Catalysis

Research Article

pubs.acs.org/acscatalysis

Reaction Pathways and Energetics of Etheric C−O Bond Cleavage Catalyzed by Lanthanide Triflates

Rajeev S. Assary,*[,†] Abdurrahman C. Atesin,[‡] Zhi Li,[‡] Larry A. Curtiss,*[,†,§] and Tobin J. Marks*[,‡]

[†]Materials Science Division and [§]Center for Nanoscale Materials, Argonne National Laboratory, Argonne, Illinois 60439, United States

[‡]Department of Chemistry, Northwestern University, Evanston, Illinois 60208, United States

Supporting Information

ABSTRACT: Efficient and selective cleavage of etheric C−O bonds is crucial for converting biomass into platform chemicals and liquid transportation fuels. In this contribution, computational methods at the DFT B3LYP level of theory are employed to understand the efficacy of lanthanide triflate catalysts ($Ln(OTf)_3$, Ln = La, Ce, Sm, Gd, Yb, and Lu) in cleaving etheric C−O bonds. In agreement with experiment, the calculations indicate that the reaction pathway for C−O cleavage occurs via a C−H → O−H proton transfer in concert with weakening of the C−O bond of the coordinated ether substrate to ultimately yield a coordinated alkenol. The activation energy for this process falls as the lanthanide ionic radius decreases, reflecting enhanced metal ion electrophilicity. Details of the reaction mechanism for $Yb(OTf)_3$-catalyzed ring opening are explored in depth, and for 1-methyl-d_3-butyl phenyl ether, the computed primary kinetic isotope effect of 2.4 is in excellent agreement with experiment (2.7), confirming that etheric ring-opening pathway involves proton transfer from the methyl group alpha to the etheric oxygen atom, which is activated by the electrophilic lanthanide ion. Calculations of the catalytic pathway using eight different ether substrates indicate that the more rapid cleavage of acyclic versus cyclic ethers is largely due to entropic effects, with the former C−O bond scission processes increasing the degrees of freedom/particles as the transition state is approached.

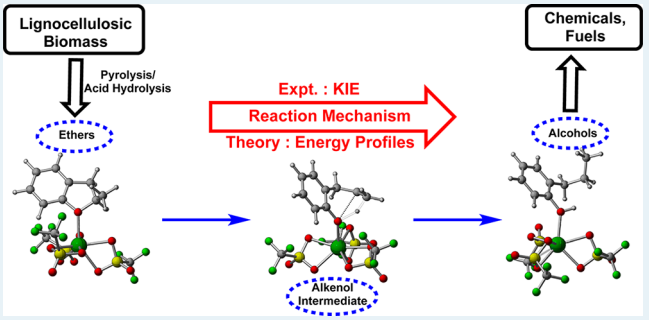

KEYWORDS: *biomass conversion, computational ether C−O hydrogenolysis, ionic liquids, lanthanide triflate catalysts, density functional theory, activation energy, kinetic isotopic effect*

1. INTRODUCTION

Due to the rapid increase in demand for transportation fuels and industrial chemicals around the globe, efficient utilization of renewable energy resources such as biomass is crucial for environmental sustainability and continued economic growth.[1−3] Ongoing research in this area during the past decade has led to significant progress in developing efficient routes for the conversion of cellulosic biomass into liquid transportation fuels and industrial chemicals via a variety of processes.[4−9] These processes, however, must be scalable and cost-effective in order for the chemical transformations of lignocellulosic materials into useful chemicals to have significant priority in our energy future.[10−16] Although thermochemical processes such as acid treatment and pyrolysis are currently available for the conversion of biomass into lower molecular weight products, they are hindered by low efficiency and poor selectivity toward desired products and are ineffective in terms of industrial level conversion of biomass to platform chemicals.[9,17−19]

Lignocellulosic biomass and the products obtained from acid-catalyzed reactions (furfurals) and fast pyrolysis (pyrans, furans) have a high oxygen content, a substantial amount of which is found as ether linkages between aliphatic, aromatic, and keto/aldehyde groups.[2] Efficient and selective cleavage of these etheric linkages would facilitate the liquification of biomass and coal into processable fuel and commodity chemical precursors.[20,21] Recently, Marks and co-workers[22] reported on a selective $Ln(OTf)_3$/Pd nanoparticle-mediated tandem catalytic etheric C−O bond hydrogenolysis process in "green" ionic liquid media.

Based on the microscopic reverse of the well-documented alkene hydroalkoxylation reaction,[23,24] this atom-economical route consists of a tandem system in which the $Ln(OTf)_3$ cleaves the etheric C−O bond through an endothermic homogeneous bond scission process (Scheme 1, Cycle A) to yield an alkenol intermediate, which then undergoes exothermic heterogeneous hydrogenation mediated by the Pd nanoparticles (Scheme 1, Cycle B). Due to the high reaction temperatures, significant deactivation of the Pd nanoparticle catalyst is observed, presumably due to agglomeration, when commercial catalysts such as Pd/C and $Pd/BaSO_4$ are used.

Received: April 24, 2013
Published: July 15, 2013

   dx.doi.org/10.1021/cs400483q | ACS Catal. 2013, 3, 1908−1914

Scheme 1. Proposed Pathway for Tandem Lanthanide Triflate/Pd Nanoparticle-Mediated Etheric C−O Bond Hydrogenolysis[a]

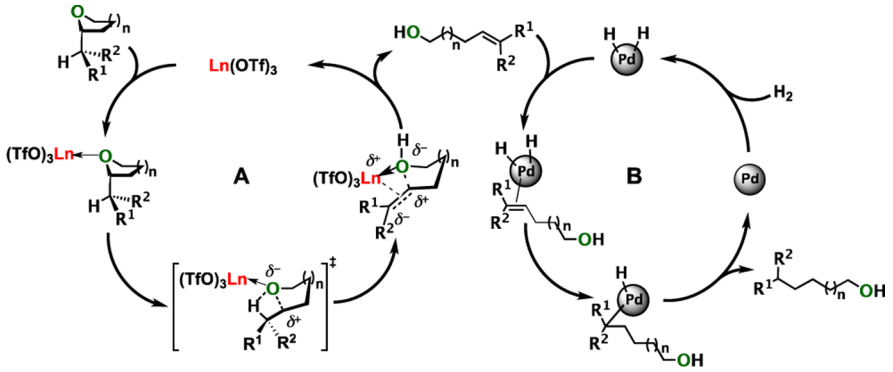

[a]Ln = lanthanide; R^1, R^2 = organic functional group. Cycle A is found to be turnover-limiting.

However, sinter-resistant Pd nanoparticles deposited on Al_2O_3 via atomic layer deposition are significantly more robust, and the hydrogenation reactions proceed to completion in this case.[25,26] In this catalytic process, it is found that the C−O bonds of acyclic ethers cleaved more rapidly than those of cyclic ethers, possibly reflecting entropic and/or steric factors. Far slower or negligible C−O cleavage is observed with substrates lacking a methyl group alpha to the etheric O atom, such as di-*n*-octylether and tetrahydropyran. This observation is in good agreement with the regiochemistry of the reverse hydroalkoxylation process (reverse of Scheme 1, Cycle A). Kinetic studies reveal that C−O bond scission is the turnover-limiting step here, with the rate law being first-order with respect to substrate and $Ln(OTf)_3$ concentration, and zero-order in hydrogen pressure.[22]

As a consequence of the endothermicity of the ring-opening process, the kinetics and thermodynamics that control rate and selectivity in the $Ln(OTf)_3$-catalyzed dehydroalkoxylation process are key features that require molecular level understanding if ever more efficient and selective catalysts are to be invented. In this contribution, we employ density functional theory at the B3LYP level to analyze mechanistic and reaction energetic trends for a series of ethers and lanthanide ions, including analysis of kinetic isotope effects.

2. COMPUTATIONAL DETAILS

All calculations described in this investigation were performed using the B3LYP[27] density functional. A 6-31+G(d) basis set was used for atoms such as C, H, O, N, S, and F. The Stuttgart RSC 1997 ECP basis set was used for Ce, Sm, Gd, Yb, and Lu atoms. The LANL2TZ(f) basis set was used for La. The basis sets for the lanthanides (Ln) were obtained from the EMSL database.[28,29] A detailed description regarding the modeling of the catalyst (Figure S1 of the Supporting Information) and reactions is presented in the Supporting Information. All structures presented in the paper are fully relaxed, and normal coordinate analysis was performed for all stationary points to characterize the transition states (one imaginary frequency) and the equilibrium structures (no imaginary frequencies) and to calculate the zero point energy correction (ZPE). To include the contributions from solvent medium in the reaction energetics (enthalpies and free energies at 298 K and 1 atm pressure), the solvation energies were computed using the SMD solvation model[30] using a dielectric medium of 2-butanol (ε = 15.9) at 298 K and using the gas phase geometry at the B3LYP level of theory. Thus, the enthalpies of activation in solution computed here include the solvation energies.[31] In addition to the B3LYP/6-31+G(d) calculations, MP2/6-311+G(2df,p)//B3LYP/6-31+G(d) level calculations were also performed for the uncatalyzed reactions to check the accuracy of B3LYP method. All calculations were performed using the G09 software.[32]

3. EXPERIMENTAL DETAILS

3.1. Materials and Methods. All manipulations of reagents were carried out under an N_2 atmosphere. $CDCl_3$ was obtained from commercial sources and stored over molecular sieves. Heptanal, CD_3MgI, phenol, triphenylphosphine, and diethyl azodicarboxylate were obtained from Aldrich Chemical Co. and used without further purification. $Yb(OTf)_3$[33] and Pd nanoparticles on alumina (Pd@ALD)[25] containing 2% Pd by weight were synthesized according to previously published procedures. The labeled substrates 1-d_3-2-octanol[34] and 1-methyl-d_3-heptyl phenyl ether[35] were synthesized according to modified literature procedures as outlined below. The ^{1}H NMR integration internal standard, 1,1,2,2-tetrachloroethane, was purchased from Aldrich Chemical Co., distilled under reduced pressure, and stored under N_2. The ionic liquid [EMIM][OTf] was prepared according to a published procedure[36] and stored under an inert atmosphere.

3.2. Physical and Analytical Measurements. NMR spectra were recorded on a Varian Inova-500 (500 MHz, ^{1}H, 100 MHz, ^{13}C) spectrometer. Chemical shifts (δ) for ^{1}H and ^{13}C are referenced to solvent peaks. A Varian 1200 Quadrupole mass spectrometer was used to obtain mass spectral data. C−O cleavage reactions were performed in a Parr reactor (model 4590, 100 mL, Parr Co., Moline, IL), capable of reaching 300 °C, 1000 psi, and a 3000 rpm stirring rate.

3.3. Preparation of 1-d_3-2-octanol. To a 3-neck round-bottom flask equipped with a condenser and magnetic stirrer was charged 50 mL of 1 M CD_3MgI in Et_2O. Heptanal (45 mmol) was added dropwise with a syringe to allow a gentle refluxing of the ether solution, which was then refluxed for 3 h prior to quenching with 100 mL of 1 M aqueous HCl. The mixture was then separated and extracted with 3 × 50 mL of Et_2O. The combined organic phase was washed with 2 × 50 mL of brine, dried with Na_2SO_4, and evaporated in vacuo. The resulting liquid was passed through a short silica gel column with 3:1 hexane/ethyl acetate mixture as the eluent. Evaporation of the solvents resulted in 1-d_3-2-octanol (5.6g, 93%). ^{1}H NMR ($CDCl_3$): δ 3.78 (m, 1 H), 1.22−1.52 (m, 10

dx.doi.org/10.1021/cs400483q | ACS Catal. 2013, 3, 1908−1914

H), 0.89 (t, J = 7.1 Hz, 3 H). ^{13}C {^{1}H} NMR ($CDCl_3$): δ 68.2, 39.5, 32.0, 29.6, 25.7, 22.8, 14.2.

3.4. Preparation of 1-Methyl-d_3-Heptyl Phenyl Ether. To a round-bottom flask were charged 1-d_3-2-octanol (42 mmol), phenol (84 mmol), triphenylphosphine (88 mmol), and THF (170 mL). The mixture was stirred for 20 min to let all solids dissolve prior to cooling to 0 °C with an ice bath. Diethyl azodicarboxylate (88 mmol) was then added very slowly at 0 °C over 20 min. The mixture was warmed to room temperature and stirred overnight. The solvent was then evaporated, and residue was redissolved in 100 mL of CH_2Cl_2. The solution was passed through a silica gel pad (11 cm diameter, 7 cm height) in a fritted funnel. The silica pad was washed with 500 mL of CH_2Cl_2, and all organics were collected and evaporated to 300 mL total volume. The solution was then washed sequentially with 300 mL each of 15% H_2O_2, saturated Na_2SO_3, and H_2O. The last H_2O wash was back extracted with 200 mL of CH_2Cl_2, and all organics were collected and dried on Na_2SO_4. The solution was then filtered through another 11 × 5 silica pad. The silica pad was washed with 5 × 200 mL of hexanes. Evaporation of all collected fractions provided the title compound (7.9g, 90%). ^{1}H NMR ($CDCl_3$): δ 7.17−7.28 (m, 2 H), 6.80−6.93 (m, 3 H), 4.25−4.35 (m, 1 H), 1.63−1.80 (m, 1 H),1.18−1.59 (m, 9 H), 0.78−0.93 (m, 3 H). ^{13}C {^{1}H} NMR ($CDCl_3$): δ 158.4, 129.5, 120.5, 116.0, 73.8, 36.6, 32.0, 29.5, 25.7, 22.8, 19.1 (m, CD_3), 14.2. ^{2}D {^{1}H} NMR ($CDCl_3$): δ 1.30.

3.5. Yb(OTf)$_3$-Mediated Reaction of 1-Methyl-d_3-heptyl Phenyl Ether in [EMIM][OTf]. Yb(OTf)$_3$ (10 mol %, 6.5 × 10^{-5} mol), Pd@ALD (1.3 × 10^{-5} mol Pd), [EMIM][OTf] (2.6 × 10^{-2} mol), and substrate (6.5 × 10^{-4} mol, 10 equiv with respect to Yb(OTf)$_3$) were added to a 100 mL Teflon sleeve and then put into the Parr reactor in a glovebox and sealed. The reactor was purged with 100 psi hydrogen 10 times, after which the reactor was heated, pressurized, and stirred at 1000 rpm for 18 h. The progress of the reaction was followed by taking aliquots during the reaction through a needle valve on the Parr reactor after cooling the reaction mixture to 80 °C and decreasing the pressure to 30 psi. Upon the completion of the reaction, the reactor was cooled down to room temperature and depressurized. The final products phenol-OD and octane-1,1-d_2 were separated from the ionic liquid by vacuum distillation. The kinetic isotope effect was calculated by measuring the initial rates of the reaction and comparing it to the protio substrate under identical reaction conditions.[22] Spectral data of phenol-OD matched those of commercially available phenol-OD. Octane-1,1-d_2: ^{1}H NMR ($CDCl_3$): δ 1.20−1.35 (m, 12 H), 0.84−0.96 (m, 4 H). ^{13}C {^{1}H} NMR ($CDCl_3$): δ 32.8, 30.5, 23.4, 22.0, 21.2, 14.1. ^{2}D {^{1}H} NMR ($CDCl_3$): δ 1.22.

4. RESULTS AND DISCUSSION

A schematic representation of the reaction coordinate and various energy terms associated with the conversion of ether to alcohol via an alkenol is shown in Scheme 2. The changes in energies of the ether, alkenol intermediate, and alcohol product when bound to the catalyst are given as ΔE in the scheme but are reported as free energies ($\Delta G°$(298 K)) and enthalpies ($\Delta H°$(298 K)) as appropriate in this section. The labels ΔE^{app} and ΔE^{int} stand for apparent and intrinsic activation energies. On the basis of the experimental kinetic results, Marks and co-workers proposed that the turnover-limiting step for the tandem ether to alcohol conversion is the cleavage of the

Scheme 2. Schematic Representation of the Catalytic Conversion of Ether to Alkenol to Alcohol through Ring Opening and Subsequent Hydrogenation[a]

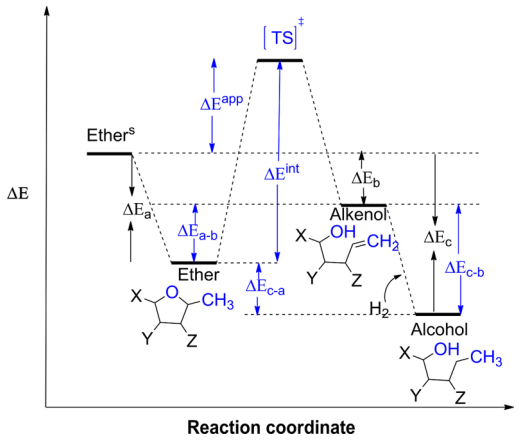

[a]The superscript "s" indicates that the ether is in solution and the rest of the species are bound to the catalyst in solution. Also shown are the various energy terms (ΔE) with respect to reaction coordinate.

etheric C−O bond. According to this mechanistic picture, the ether molecule binds to the metal center (Ln^{3+}) through the electron-rich oxygen, followed by a proton transfer from the α-methyl group to the etheric oxygen to form an alkenol intermediate. Subsequent hydrogenation results in the formation of saturated alcohols.

Experimentally, it is observed that the catalytic activity of the lanthanide triflates increases as the ionic radius of the Ln^{3+} ion decreases (Lewis acidity increases[37]). To acquire a better theoretical understanding of this observation, we chose La(OTf)$_3$, Ce(OTf)$_3$, Sm(OTf)$_3$, Gd(OTf)$_3$, Yb(OTf)$_3$, and Lu(OTf)$_3$ as catalyst models and computed their energetics and reaction barriers for C−O bond cleavage. Optimized structures of the metal triflates, complexes of metal triflates with ether, alkenol, and alcohol, and the transition state structure for the C−O bond cleavage are presented in the Supporting Information. The ether substrate, 2,3-dihydro-2-methylbenzofuran, **1A**, was chosen to understand details of the energy profile along the reaction coordinate to alkenol (**1B**) and subsequent hydrogenation to afford *n*-propyl phenol (**1C**) (eq 1).

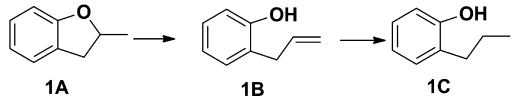

(1)

Since Ln(III) triflates have differing solvation energies, we have also incorporated the solvation energetics in this study. Two important parameters were considered and computed: the intrinsic enthalpy of activation (shown in Scheme 2, ΔH^{int}) and the free energy of reaction ($\Delta G_{b\text{-}c}$) from the Ln(OTf)$_3$ coordinated ether to alkenol. The catalytic reactions that require a relatively low activation enthalpy and have a negative free energy for the ether to alkenol conversion are considered to be most likely. Following the aforementioned criterion, the enthalpy of activation for the etheric C−O bond cleavage of **1A** using various Ln(OTf)$_3$ catalysts and the free energy change for the ether-alkenol reaction were computed. The results of these calculations are shown in Figure 1. Details of the computed enthalpy parameters in gas phase and in solution can be found

dx.doi.org/10.1021/cs400483q | ACS Catal. 2013, 3, 1908−1914

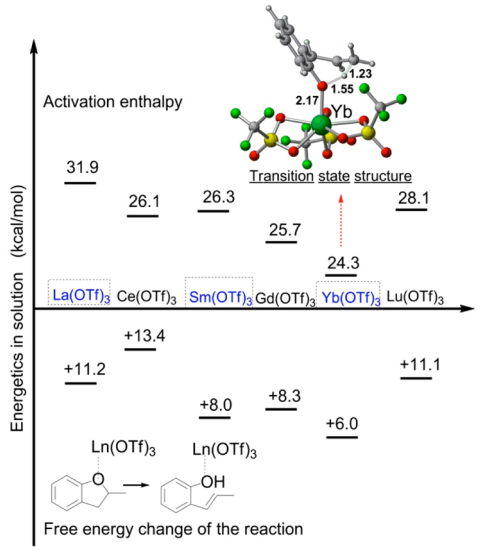

Figure 1. Computed enthalpy barriers (top) and free energies for the conversion of ether to enol catalyzed by various $Ln(OTf)_3$ (Ln = La, Ce, Sm, Gd, Yb, and Lu) catalysts in solution. All energies were computed at the B3LYP level of theory. Under identical reaction conditions, the experimental turnover frequencies of catalysts $La(OTf)_3$, $Sm(OTf)_3$, and $Yb(OTf)_3$ are 0.12, 0.22, and 0.55 h^{-1}, respectively.[22]

in Table S1 of the Supporting Information. The $Ln(OTf)_3$ cases for which there is experimental data are highlighted with a rectangular box, ($Yb(OTf)_3$, $Sm(OTf)_3$, and $La(OTf)_3$).

Optimized geometries and gas phase enthalpy profiles for the lanthanide triflates can be found in Figures S3–S6 of the Supporting Information. Based on the computed activation enthalpies and the reaction free energies associated with the **1A** → **1B** conversion, $Yb(OTf)_3$ is found to be the most active catalyst among the various $Ln(OTf)_3$ catalytic models examined in this comparison. The computed activation enthalpy for the **1A** → **1B** cleavage by Yb^{3+} is 24.3 kcal/mol, in contrast to the uncatalyzed reaction that has an activation barrier of 56 kcal/mol (see Figure S2, Supporting Information), and the reaction is calculated to be endergonic by 6 kcal/mol. In terms of the reaction barriers, $Ce(OTf)_3$, $Sm(OTf)_3$, and $Gd(OTf)_3$ show similar intrinsic enthalpic barriers (~26 kcal/mol) for the reaction, while both the $La(OTf)_3$- and $Lu(OTf)_3$-catalyzed reactions require relatively higher barriers of 32 and 28 kcal/mol, respectively. In terms of free energies of reaction, the $La(OTf)_3$-, $Lu(OTf)_3$-, and $Ce(OTf)_3$-catalyzed reactions are slightly more endergonic versus the $Yb(OTf)_3$-, $Sm(OTf)_3$-, and $Gd(OTf)_3$-catalyzed reactions. The activity of the catalysts increases with the increase of the charge density and the decrease of the ionic radius of the central metal ions. Note that a direct correlation between the Ln^{3+}–O_{ether} bond distances (optimized geometry) and the ionic radii/charge density of the Ln^{3+} ions is observed (Table 1). This computed trend in lanthanide catalytic activities is consistent with the experimental results of Marks and co-workers, where they investigated $Yb(OTf)_3$, $Sm(OTf)_3$, and $La(OTf)_3$ for the cleavage of the **1A** etheric bond.[22] A trend of decreasing activation barrier with decreasing Ln^{3+} ionic radius and Ln^{3+}–O_{ether} bond length is observed in the lanthanide-catalyzed ether ring opening.[22] We speculate that the increase in charge density of the central cation (upon lanthanide contraction) results in an increased Lewis acidity, which could be the reason for the effective

Table 1. Comparison of Ionic Radii and Computed Ln^{3+}–O_{Ether} Bond Lengths (Å) for Various Ln^{3+} Ions and $Ln(OTf)_3$ Complex with the Ethers

	La	Ce	Sm	Gd	Yb	Lu
ionic radius (Å)	1.03	1.01	0.96	0.94	0.87	0.86
APT charge[a] (e)	2.68	2.69	2.61	2.59	2.44	2.41
charge density	2.60	2.66	2.72	2.77	2.81	2.80
Ln^{3+}–O_{ether} (Å)	2.62	2.58	2.47	2.44	2.38	2.35

[a]Atomic polar tensor (APT) charges are obtained from DFT frequency calculations.

activation of etheric bond and subsequent proton transfer to cleave the etheric C–O bond. This is partially supported by the increase in computed charge density (Table 1) of various Ln^{3+} ions in $Ln(OTf)_3$ with the decrease of effective ionic radii.

To probe the proposed mechanistic scenario outlined in Schemes 1 and 2, kinetic isotope effect data were obtained for the cleavage of the etheric C–O bond in 1-methyl-d_3-heptyl phenyl ether by ^{1}H NMR spectroscopy (Ph-O-C(H)(R)-CH_3 vs Ph-O-C(H)(R)-CD_3). These experiments yielded a k_H/k_D of 2.7, which is suggestive of a primary KIE. Next, 1-methylbutyl phenyl ether, **8A**, was used in the calculations to compare with the experimentally obtained value. The detailed enthalpy landscape in the gas phase for the conversion of this ether to alcohol is shown in Figure 2. The computed intrinsic activation

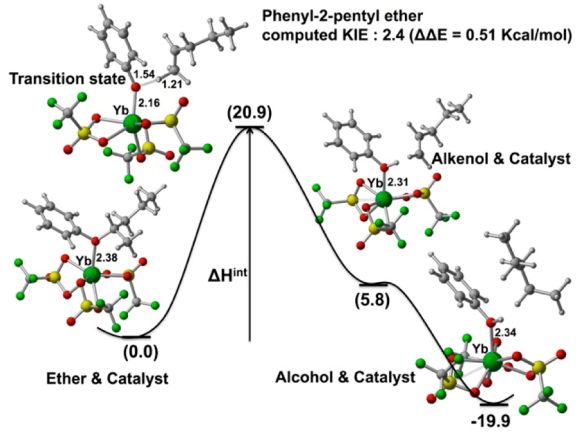

Figure 2. Computed gas phase enthalpy profile for the conversion of **8A** to pentane and phenol catalyzed by $Yb(OTf)_3$ at the B3LYP level of theory.

enthalpy required for the C–O bond cleavage of **8A** is 20.9 kcal/mol. The ring cleavage process yields 1-pentene and a $Yb(OTf)_3$-phenol complex. This reaction is computed to be endothermic by 5.8 kcal/mol, while the subsequent hydrogenation of 1-pentene is exothermic by 19.9 kcal/mol. Experimentally, Pd nanoparticles are reported to catalyze the hydrogenation reaction, as noted above. For computational simplicity, the decomplexation kinetics of alkene and phenol from the Yb^{3+} center and the subsequent energetics of hydrogenation by the Pd nanoparticles were not computed.

The computed activation energy differences ($\Delta\Delta E^{TS}$(H/D)) between the α-CH_3 and the α-CD_3 derivatives of phenyl-2-pentyl ether is 0.51 kcal/mol; the details of the KIE evaluation are presented in Scheme S1 and Table S2 of the Supporting Information. This small change in energy corresponds to a KIE for proton transfer of 2.4, which is in excellent agreement with the experimental value of 2.7.

dx.doi.org/10.1021/cs400483q | ACS Catal. 2013, 3, 1908–1914

Figure 3 shows the gas phase enthalpy profile associated with the ring opening and subsequent hydrogenation of **1A** to **1C**. In

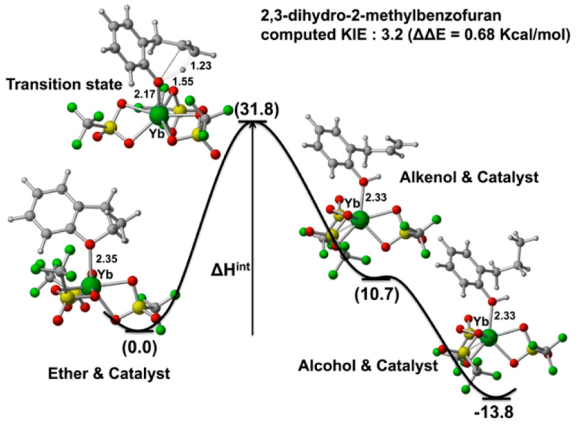

Figure 3. Computed gas phase enthalpic profile for the conversion of 2,3-dihydro-2-methylbenzofuran (**1A**) to propyl phenol catalyzed by $Yb(OTf)_3$ at the B3LYP level of theory.

the gas phase, binding of the ether through its oxygen atom to $Yb(OTf)_3$ is an exothermic process (−14 kcal/mol, not shown), and the intrinsic activation enthalpy for ring opening (ether to TS) is +31.8 kcal/mol. Note that conversion of the ether to alkenol is an endothermic process (+10.7 kcal/mol), while the subsequent hydrogenation (alkenol to alkanol) is exothermic (−24.5 kcal/mol). The computed activation energy differences ($\Delta\Delta E^{TS}$(H/D)) between the α-CH_3 and the α-CD_3 derivatives of **1A** is 0.67 kcal/mol, with the details of the KIE evaluation presented in the Table S2 of the Supporting Information. This small change in energy corresponds to a KIE for proton transfer of 3.2 (see Table S2 of the Supporting Information). Although we have not measured the experimental KIE for this substrate, the computed KIE suggests a proton transfer pathway similar to that of **8A**.

Comparing the ring opening of **8A** to that of **1A**, it can be seen that the linear ether incurs a smaller barrier (20.9 kcal/mol) and that the C−O bond cleavage reaction is less endergonic (+5.8 kcal/mol) when compared to the corresponding parameters for **1A**, 31.8 and 10.7 kcal/mol, respectively. These results indicate that the catalytic reaction of linear ethers is kinetically and thermodynamically more favorable than for the cyclic ethers. Experimentally, it is found that linear ethers are more rapidly cleaved than cyclic ethers, requiring lower temperatures for the corresponding reactions to proceed to completion (110 vs 180 °C).[22]

A total of eight etheric substrates that have been studied by Marks and co-workers were next selected in order to compute the energetics of the ring opening and subsequent hydrogenation processes as shown in Figure 4. All the substrates have a methyl substituent at the α-position to the etheric oxygen atom. Detailed gas phase thermochemistry including reaction barriers were computed at the B3LYP/6-31+G(d) level of theory (gas phase) for the uncatalyzed C−O bond cleavage and subsequent hydrogenation reactions. This level of theory provides reasonably good agreement compared to a MP2/6-311+G(3df,2p)//B3LYP/6-31+G(d) level of calculation in predicting most of the reaction energetics and reaction barriers (see Figure S7 in the Supporting Information). Exceptions are the barriers for the C−O bond-breaking reactions in ethers **1A** and **5A** (Figure 4). These substrates have a phenyl group

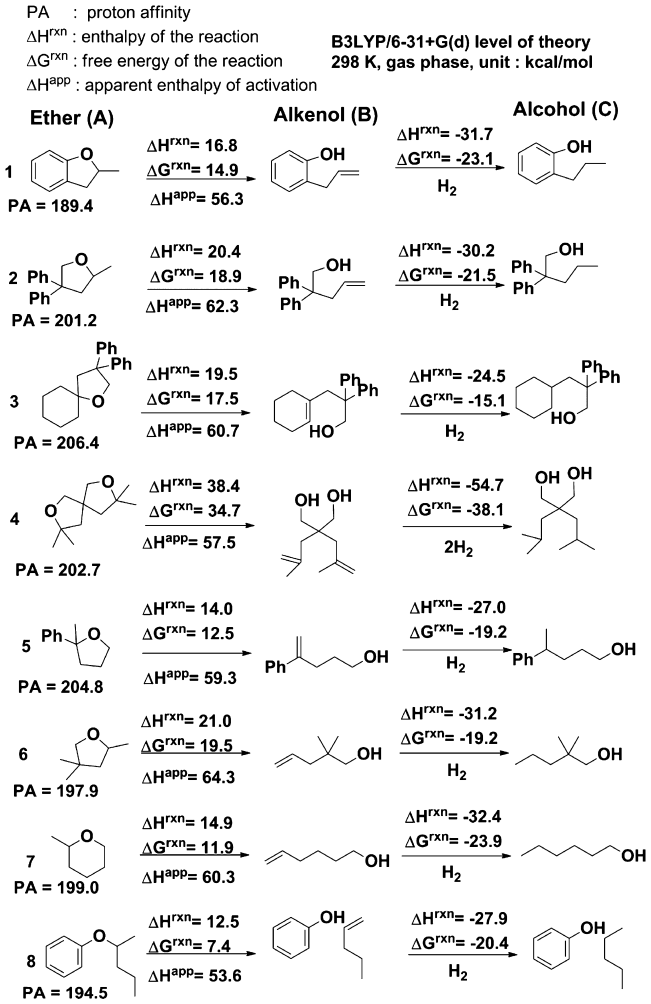

Figure 4. Computed energetics of uncatalyzed conversion of ether to alcohol in the gas phase at the B3LYP/6-31+G(d) level of theory. Note that for substrate **4** the computed reaction barrier is for breaking one C−O bond, but reaction energies are for two bonds.

adjacent to the etheric oxygen, and density functional theory underestimates the reaction barriers by ∼10 kcal/mol.

These calculations clearly indicate that the ring opening is endothermic for all substrates (12−21 kcal/mol), while hydrogenation of the corresponding alkenols is exothermic ((−24 to −32 kcal/mol; Table S1 of the Supporting Information). In terms of the reaction barriers for the uncatalyzed reactions, the formation of the alkenol intermediates from the ether species invariably incurs an activation barrier ($\Delta H^{int} = \Delta H^{app}$) of about 60 kcal/mol. The formation of alkenol in the gas phase is found to take place via proton transfer (Figure S2 of the Supporting Information), and the computed barrier is extremely high, indicating that these reactions are kinetically not feasible. Another essential parameter that was computed is the proton affinities of oxygen atoms (PA) of the substrates, for which the computed values range from 190 to 206 kcal/mol, depending on the substituents around the etheric oxygen atom. Note that the PAs of the ethers increase in the presence of electron-donating substituents (methyl or alkyl groups) adjacent to the ether oxygen. It is therefore likely that substrates with higher proton affinities would interact with the positively charged lanthanide ions (Ln^{3+}) more strongly than the substrates with lower proton

dx.doi.org/10.1021/cs400483q | ACS Catal. 2013, 3, 1908−1914

affinities. A stronger interaction suggests an effective Lewis "adduct" between the metal ion (Lewis acid) and the etheric oxygen (Lewis base) and subsequent activation of the C−O bond is likely to be determined by the Lewis basicity of various metal ions (Lewis acid).

The computed intrinsic activation enthalpies, free energy changes for the catalyzed conversion of the ethers to alkenols, and the enthalpies of binding the ether substrates to $Yb(OTf)_3$ are summarized in Figure 5. Detailed relative free energies of

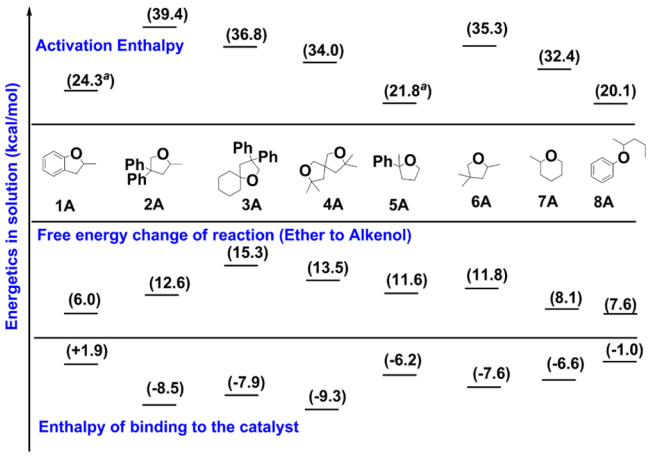

Figure 5. Computed enthalpic barriers (top), free energies (middle) for the conversion of ether to alkenol catalyzed by $Yb(OTf)_3$, and enthalpies of binding of the ether substrates to the catalyst (bottom) in solution at the B3LYP level of theory. Various ethers (**1A**−**8A**) are shown in Figure 4.

ethers, alkenols, and alkanols can also be found in Table S3 of the Supporting Information. From Figure 5, it is evident that the computed activation enthalpies for all the substrates are below 40 kcal/mol. Since the uncatalyzed reactions have an activation barrier of ∼60 kcal/mol (Figure 4), it is clear that $Yb(OTf)_3$ substantially lowers the barriers for all the ether substrates.

Two ether substrates that show quantitatively lower activation enthalpies are **1A** and **5A**. For these two species, which have phenyl groups adjacent to the etheric oxygen, note that the B3LYP level of theory underestimates the reaction barriers compared to the MP2 level of theory (Figure S7). As noted above, experimental kinetic measurements show that linear ethers such as **8A** undergo more rapid ring opening than cyclic ethers. The calculations presented here are consistent with these observations, indicating that **8A** incurs a relatively low activation barrier compared to cyclic ethers **1A**−**7A**. This is consistent with expected entropic effects due to the increased number of particles/degrees of freedom accompanying the scission of the C−O bonds in linear ethers.

5. CONCLUSIONS

Selective and efficient cleavage of etheric C−O bonds is an important challenge in future processes for the conversion of biomass to platform chemicals. The selective tandem catalytic $Ln(OTf)_3$/Pd nanoparticle-mediated etheric C−O bond hydrogenolysis process in ionic liquids represents a new approach. In this paper, detailed computational studies were performed to screen the activities of various lanthanide triflates toward C−O bond cleavage. The density functional studies (B3LYP) suggest that the activity of catalysts increases as the ionic radius of the central metal ion decreases. $Yb(OTf)_3$ was found to be the most effective catalyst among the various lanthanide triflates considered in this investigation. The detailed reaction mechanism of the $Yb(OTf)_3$-catalyzed ether ring opening was explored by measurement of the KIE using both experiment and density functional theory. The measured KIE for phenyl-2-octyl ether (2.7) and computed KIE for phenyl-2-pentyl-ether (2.4) are in excellent agreement, indicating that the etheric ring opening occurs via a proton transfer from the α-CH_3 group upon activation of the etheric oxygen by the electrophilic metal ion. Based on the concept of this activation of ether oxygen atoms, we speculate that the metal ions with higher positive charge density (M^{4+} ions, small M^{3+} ions) would be ideal candidates for more efficient C−O bond-breaking catalysts, which require future experimental and theoretical investigations. Calculations using various ethers suggest that the C−O bonds of linear ethers cleaved more rapidly than those of cyclic ethers, consistent with the increase in entropy due to the increase in the number of particles/degrees of freedom from the scission of the C−O bond.

■ ASSOCIATED CONTENT

Supporting Information

Details of computations, enthalpy profiles for the liquid phase $Ln(OTf)_3$-catalyzed hydrogenolysis of **1A** ether (Ln = La, Ce, Sm, Gd), enthalpy profile for gas phase C−O cleavage of **1A**. Details of KIE and MP2 energetics for the uncatalyzed reactions of ethers **1A**−**8A**. This material is available free of charge via the Internet at http://pubs.acs.org.

■ AUTHOR INFORMATION

Corresponding Author

*E-mail: assary@anl.gov; curtiss@anl.gov; t-marks@northwestern.edu.

Notes

The authors declare no competing financial interest.

■ ACKNOWLEDGMENTS

This work was supported by the U.S. Department of Energy under contract DE-AC0206CH11357. This material is based upon work supported as part of the Institute of Atom Efficient Chemical Transformation (IACT), an Energy Frontier Research Center funded by the U.S. Department of Energy, Office of Sciences, and Office of Basic Energy Sciences. We gratefully acknowledge the computing resources provided on "Fusion", a 320-node computing cluster operated by the Laboratory Computing Resource Center at Argonne National Laboratory. Use of the Center for Nanoscale Materials was supported by the U.S. Department of Energy, Office of Science, Office of Basic Energy Sciences, under Contract No. DE-AC02-06CH11357. This research also used resources of the National Energy Research Scientific Computing Center (NERSC), which is supported by the Office of Science of the U.S. Department of Energy under Contract No. DE-AC02-05CH11231. We also acknowledge grants of computer time from EMSL, a national scientific user facility located at the Pacific Northwest National Laboratory. Z.L. was supported under NSF grant CHE-1213235 on basic f-element chemistry, which also provided necessary equipment.

■ REFERENCES

(1) Regalbuto, J. R. *Science* **2009**, *325*, 822.

(2) Corma, A.; Iborra, S.; Velty, A. *Chem. Rev.* **2007**, *107*, 2411.
(3) Huber, G. W.; Iborra, S.; Corma, A. *Chem. Rev.* **2006**, *106*, 4044.
(4) Chheda, J. N.; Huber, G. W.; Dumesic, J. A. *Angew. Chem., Int. Ed.* **2007**, *46*, 7164.
(5) Bond, J. Q.; Alonso, D. M.; Wang, D.; West, R. M.; Dumesic, J. A. *Science* **2010**, *327*, 1110.
(6) Huber, G. W.; Chheda, J. N.; Barrett, C. J.; Dumesic, J. A. *Science* **2005**, *308*, 1446.
(7) Kunkes, E. L.; Simonetti, D. A.; West, R. M.; Serrano-Ruiz, J. C.; Gartner, C. A.; Dumesic, J. A. *Science* **2008**, *322*, 417.
(8) van Putten, R.-J.; van der Waal, J. C.; de Jong, E.; Rasrendra, C. B.; Heeres, H. J.; de Vries, J. G. *Chem. Rev.* **2013**, *11*, 1499.
(9) Lange, J.-P.; Price, R.; Ayoub, P. M.; Louis, J.; Petrus, L.; Clarke, L.; Gosselink, H. *Angew. Chem., Int. Ed.* **2010**, *49*, 4479.
(10) Bozell, J. J.; Petersen, G. R. *Green Chem.* **2010**, *12*, 539.
(11) Lange, J.-P.; van der Heide, E.; van Buijtenen, J.; Price, R. *ChemSusChem* **2012**, *5*, 150.
(12) Bermejo-Deval, R.; Assary, R. S.; Nikolla, E.; Moliner, M.; Roman-Leshkov, Y.; Hwang, S.-J.; Palsdottir, A.; Silverman, D.; Lobo, R. F.; Curtiss, L. A.; Davis, M. E. *Proc. Natl. Acad. Sci. U.S.A.* **2012**, *109*, 9727.
(13) Zhang, Z.; Dong, K.; Zhao, Z. *ChemSusChem* **2011**, *4*, 112.
(14) Gonzalez Maldonado, G. M.; Assary, R. S.; Dumesic, J.; Curtiss, L. A. *Energy Environ. Sci.* **2012**, *5*, 6981.
(15) Gonzalez Maldonado, G. M.; Assary, R. S.; Dumesic, J. A.; Curtiss, L. A. *Energy Environ. Sci.* **2012**, *5*, 8990.
(16) Zhao, H.; Holladay, J. E.; Brown, H.; Zhang, Z. C. *Science* **2007**, *316*, 1597.
(17) Geboers, J. A.; Van de Vyver, S.; Ooms, R.; Op de Beeck, B.; Jacobs, P. A.; Sels, B. F. *Catal. Sci. Technol.* **2011**, *1*, 714.
(18) Van de Vyver, S.; Geboers, J.; Jacobs, P. A.; Sels, B. F. *ChemCatChem* **2011**, *3*, 82.
(19) Van de Vyver, S.; Thomas, J.; Geboers, J.; Keyzer, S.; Smet, M.; Dehaen, W.; Jacobs, P. A.; Sels, B. F. *Energy Environ. Sci.* **2011**, *4*, 3601.
(20) Zakzeski, J.; Bruijnincx, P. C. A.; Jongerius, A. L.; Weckhuysen, B. M. *Chem. Rev.* **2010**, *110*, 3552.
(21) Climent, M. J.; Corma, A.; Iborra, S. *Green Chem.* **2011**, *13*, 520.
(22) Atesin, A. C.; Ray, N. A.; Stair, P. C.; Marks, T. J. *J. Am. Chem. Soc.* **2012**, *134*, 14682.
(23) Dzudza, A.; Marks, T. J. *Org. Lett.* **2009**, *11*, 1523.
(24) Dzudza, A.; Marks, T. J. *Chem.—Eur. J.* **2010**, *16*, 3403.
(25) Lu, J.; Stair, P. C. *Langmuir* **2010**, *26*, 16486.
(26) Elam, J. W.; Zinovev, A.; Han, C. Y.; Wang, H. H.; Welp, U.; Hryn, J. N.; Pellin, M. J. *Thin Solid Films* **2006**, *515*, 1664.
(27) Becke, A. D. *J. Chem. Phys.* **1993**, *98*, 1372.
(28) Feller, D. *J. Comput. Chem.* **1996**, *17*, 1571.
(29) Schuchardt, K. L.; Didier, B. T.; Elsethagen, T.; Sun, L.; Gurumoorthi, V.; Chase, J.; Li, J.; Windus, T. L. *J. Chem. Inf. Model.* **2007**, *47*, 1045.
(30) Marenich, A. V.; Cramer, C. J.; Truhlar, D. G. *J. Phys. Chem. B* **2009**, *113*, 6378.
(31) Assary, R. S.; Curtiss, L. A. *Energy Fuels* **2012**, *26*, 1344.
(32) Frisch, M. J.; Trucks, G. W.; Schlegel, H. B.; Scuseria, G. E.; Robb, M. A.; Cheeseman, J. R.; Montgomery, J. A.; Vreven, T.; Kudin, K. N.; Burant, J. C.; Millam, J. M.; Iyengar, S. S.; Tomasi, J.; Barone, V.; Mennucci, B.; Cossi, M.; Scalmani, G.; Rega, N.; Petersson, G. A.; Nakatsuji, H.; Hada, M.; Ehara, M.; Toyota, K.; Fukuda, R.; Hasegawa, J.; Ishida, M.; Nakajima, T.; Honda, Y.; Kitao, O.; Nakai, H.; Klene, M.; Li, X.; Knox, J. E.; Hratchian, H. P.; Cross, J. B.; Bakken, V.; Adamo, C.; Jaramillo, J.; Gomperts, R.; Stratmann, R. E.; Yazyev, O.; Austin, A. J.; Cammi, R.; Pomelli, C.; Ochterski, J. W.; Ayala, P. Y.; Morokuma, K.; Voth, G. A.; Salvador, P.; Dannenberg, J. J.; Zakrzewski, V. G.; Dapprich, S.; Daniels, A. D.; Strain, M. C.; Farkas, O.; Malick, D. K.; Rabuck, A. D.; Raghavachari, K.; Foresman, J. B.; Ortiz, J. V.; Cui, Q.; Baboul, A. G.; Clifford, S.; Cioslowski, J.; Stefanov, B. B.; Liu, G.; Liashenko, A.; Piskorz, P.; Komaromi, I.; Martin, R. L.; Fox, D. J.; Keith, T.; Laham, A.; Peng, C. Y.; Nanayakkara, A.; Challacombe, M.; Gill, P. M. W.; Johnson, B.; Chen, W.; Wong, M. W.; Gonzalez, C.; Pople, J. A. *Gaussian 09, Rev. C.01*; Gaussian, Inc.: Wallingford CT, 2009.
(33) Dzudza, A.; Marks, T. J. *J. Org. Chem.* **2008**, *73*, 4004.
(34) Stein, A. R. *Can. J. Chem.* **1994**, *72*, 1789.
(35) Proctor, A. J.; Beautement, K.; Clough, J. M.; Knight, D. W.; Li, Y. *Tetrahedron Lett.* **2006**, *47*, 5151.
(36) Bonhôte, P.; Dias, A.-P.; Papageorgiou, N.; Kalyanasundaram, K.; Grätzel, M. *Inorg. Chem.* **1996**, *35*, 1168.
(37) Cotton, A. F.; Wilkinson, G.; Murillo, C. A.; Bochmann, M. *Advanced Inorganic Chemistry*, 6th ed.; Wiley: New York, 1999.